Mechanism of Actin-Based Motility: A Dynamic State Diagram

Anne Bernheim-Groswasser,* Jacques Prost,† and Cécile Sykes†
*Chemical Engineering Department, Ben-Gurion University, Beer-Sheva, Israel; and †Laboratoire Physicochimie "Curie", UMR 168, Institut Curie/Centre National de la Recherche Scientifique, Paris, France

ABSTRACT Cells move by a dynamical reorganization of their cytoskeleton, orchestrated by a cascade of biochemical reactions directed to the membrane. Designed objects or bacteria can hijack this machinery to undergo actin-based propulsion inside cells or in a cell-like medium. These objects can explore the dynamical regimes of actin-based propulsion, and display different regimes of motion, in a continuous or periodic fashion. We show that bead movement can switch from one regime to the other, by changing the size of the beads or the surface concentration of the protein activating actin polymerization. We experimentally obtain the state diagram of the bead dynamics, in which the transitions between the different regimes can be understood by a theoretical approach based on an elastic force opposing a friction force. Moreover, the experimental characteristics of the movement, such as the velocity and the characteristic times of the periodic movement, are predicted by our theoretical analysis.

INTRODUCTION

Eukaryotic cells move by a complex mechanism of extension and retraction controlled by the cytoskeleton dynamical assembly. During locomotion, cells extend protrusions at their leading edge, and form lamellipodia and filopodia, by rearranging their actin cytoskeleton. Active sites generate, at the plasma membrane, a polarized array of actin filaments that drives the membrane protrusions. Based on a similar molecular mechanism is the intracellular propulsion of lipid vesicles (1) and endosomes (2), and certain bacterial pathogens such as *Listeria monocytogenes* (3) and *Shigella flexneri* (4). In cell movement or in the movement of these vesicles or bacteria, the same or similar proteins are the key players for motility based on actin. Site-directed actin polymerization is induced at their surfaces, via the activation of the Arp2/3 complex by WASp (Wiskott-Aldrich Syndrome protein) family proteins (5) or by bacterial proteins (i.e., ActA for *Listeria monocytogenes*) (6). This spatially controlled polymerization results in the creation of a comet tail made of a dense actin gel. The force generated by the directionality of the actin filament growth is sufficient to propel these species.

The challenge in understanding the physical mechanism of force generation by actin assembly has given rise to various theoretical descriptions (7–12). For many years *Listeria monocytogenes* was used as a model system for studying the biochemistry of actin-based movement (3) and the effect of external influences on its movement (13). *Listeria* move at a velocity of a few μm/min, either smoothly or in a periodic fashion, as observed sometimes for wild-type bacteria (14) or genetically modified bacteria (15). However, the use of *Listeria* for testing theoretical models suffers from the drawback that geometrical parameters such as its size and shape are predetermined, and that the surface density of the Arp2/3 complex bacterial activator (ActA) is unknown. Biophysical studies on movement induced by actin polymerization were greatly facilitated by the development of in vitro systems that explore actin-driven motility of non-biological cargos such as protein-coated beads (16) and lipid vesicles (17,18) placed in cell extracts. The discovery of the minimal set of proteins needed for reconstituting the movement of *Listeria* (19) opened the way for a controlled study of the physical parameters involved in actin-based motility (20). Such a system enables a detailed analysis of the physical parameters that govern actin-based movement. It was already experimentally demonstrated that at a fixed surface density of the actin polymerization activator, the type of movement is dramatically affected by changing the microsphere diameter, shifting it from a continuous to a jerky movement which resembles that of the mutated hopping *Listeria* (15).

In the work presented here, we investigate experimentally the bead diameter-protein surface density parameter space. Previously, only the influence of bead diameter was investigated in detail (20). We show that the transition from continuous to periodic regimes of motion can be induced simply by increasing the activating protein surface density as well as increasing the bead diameter. We further provide a scaling analysis of the transition from continuous to periodic regimes, and of the characteristics of this periodic regime. This analysis extends previous published works (10,21) that only provided numerical results relevant to the *Listeria* geometry. Here, we provide scaling guidelines for locating the transition from continuous to periodic behaviors and for characterizing the periodic regime. We finally compare these expectations to experimental results.

Submitted November 5, 2004, and accepted for publication May 17, 2005.

Address reprint requests to Cécile Sykes, Tel.: 33-1-423-46790; E-mail: cecile.sykes@curie.fr.

0006-3495/05/08/1411/09 $2.00

doi: 10.1529/biophysj.104.055822

MATERIALS AND METHODS

Subdomains of the Wiskott-Aldrich Syndrome protein (WASP) and their purification

Two similar subdomains of WASP know as VCA and WA were bacterially expressed as GST fusion proteins as described in Bernheim-Groswasser et al. (20) for VCA and Fradelizi et al. (22) for WA.

Protein coating of polystyrene beads

Polystyrene beads of diameter ranging from 1 to 9.1 μm were purchased from Polyscience (Niles, IL). The error bars in bead diameter were given by the manufacturer (see Table 1). We varied the protein concentration on the surface by changing the protein concentration in the incubating solution. The beads were incubated in the protein solution at concentrations in the range of 0.01–1 mg/ml for 1 h at room temperature. We used an initial volume of beads that was proportional to the diameter, i.e., volumes of 1 μl and 10 μl for beads of 1 μm and 10 μm diameters, respectively, given that the volume fraction of the beads in the stock solution was constant, equal to 2.5%. The beads were finally resuspended in a constant total volume of 20 μl to ensure a constant total surface area independently of the bead diameter. The beads were stored at 4°C in a storage buffer (20 mM phosphate buffer pH = 7.4, 150 mM NaCl, 1.5 mM NaN_3, 10 mg/ml BSA, 5% glycerol) for up to 1 week.

Determination of the surface density of VCA proteins on the bead surface

The concentration of immobilized VCA was evaluated by SDS-PAGE analysis on washed VCA-coated beads heat-denatured in SDS. To determine the surface concentration C_s of actually active proteins, we used a pyrenyl-actin polymerization assay (20). Briefly, beads carrying different surface densities of VCA were placed in a solution containing 2.5 μM G-actin (10% pyrenyl-labeled) and 20 nM Arp2/3. A calibration was first obtained using known concentrations of soluble VCA. The concentration of active immobilized VCA on beads was determined by comparison with the polymerization rate of soluble VCA. Whereas the saturating conditions lead to a 1:1 ratio of active proteins, decreasing the surface concentrations resulted in decreasing the number of active proteins on the surface. As a result, the solution concentration of 0.2, 0.05, 0.035, and 0.02 mg/ml of proteins in the incubation solution corresponds respectively to concentrations C_s of (6 ± 1), (2.2 ± 0.3), (1.17 ± 0.02), $(0.14 \pm 0.02) \times 10^{-2}$ mol/nm^2 active proteins on the bead surface. The error on the surface concentration measurement is of the order of 20% and includes bead loss in the bead-coating process due to repeated washing.

Motility assay

The motility medium contained 8.5 mM HEPES, pH = 7.7, 1.7 mM Mg-ATP, 5.5 mM DTT, 0.12 mM Dabco, 0.1 M KCl, 1 mM $MgCl_2$, 6.5 μM F-actin, 0.1 μM Arp2/3 complex, 0.046 μM capping proteins, 2.5 μM ADF, 2.5 μM profilin, 0.54 μM α-actinin, 0.31% methyl-cellulose, 0.75% BSA, and 1.1 μM actin-rhodamin as optimized for *Listeria* movement (19). No vasodilator-stimulated phosphoprotein (VASP) was needed. A 0.3-μl volume of bead suspension was added to 20 μl of motility medium. The small volume of the beads ensured that the composition of the motility medium remained unchanged. The sample was placed immediately between a glass slide and an 18-mm-square glass coverslip sealed with vaseline/lanolin/paraffin (at weight ratio of 1:1:1). To prevent squeezing of the objects, the distance between slide and coverslip was controlled using an inert polyethylene-glycol spacer (Goodfellow, Berwyn, PA) to obtain a ratio between sample height and bead diameter of 5:6. This ratio was found to ensure that the beads with their comets do not stick to the coverslip walls. In all experiments, symmetry breaking occurs spontaneously and 100% of the beads generate a comet.

Tracking and imaging of bead movement

The characterization of the bead movement, polymerization dynamics, and comet structure were performed by means of phase contrast and fluorescence microscopy techniques (Olympus IX51 microscope, Melville, NY). Each data point was obtained by averaging experimental data from a minimum of 10 beads. The movement of the microspheres was tracked during 1.5 h by timelapse optical video-microscopy. Measurement of the beads velocity was performed as in Bernheim-Groswasser et al. (20). The thickness of the actin gel in the comet of saltatory moving beads was determined as the distance between the inflection points in the gray-level intensity curve obtained as a linescan of the middle of the comet.

RESULTS

Transition from continuous to saltatory movement

Beads of 1–9.1-μm diameter were grafted at different surface densities C_s of VCA or WA subdomain (C_s, concentration of active proteins, from 0.14 to 6×10^{-2} molecules/nm^2, see Materials and Methods, above). Once placed in the motility medium, these beads started to assemble an actin gel, resulting in a homogeneous, spherical actin cloud around the bead. In a time ranging from 3 to 25 min, the spherical

TABLE 1

Beads diameter (μm)	t_s (min)	τ' (min)	τ_{rep} (min)	τ (min)	τ_{rep}/τ'	τ/τ'
0.954 ± 0.028	n.d.	n.d.	n.d.	n.d.	n.d.	n.d.
2.134 ± 0.039	n.d.	n.d.	n.d.	n.d.	n.d.	n.d.
2.837 ± 0.133	11 ± 1.8	13.5 ± 2.4	9.1 ± 2.7	1.15 ± 0.54	0.75 ± 0.06	0.095 ± 0.034
4.537 ± 0.236	13.5 ± 2	9.9 ± 1.3	7.2 ± 1.8	0.78 ± 0.20	0.81 ± 0.06	0.83 ± 0.016
6.348 ± 0.455	14.7 ± 1.1	8.5 ± 0.72	4.8 ± 0.41	1.37 ± 0.61	0.57 ± 0.04	0.16 ± 0.081
9.14 ± 0.709	24.4 ± 5.0	7.2 ± 1.3	4.3 ± 0.61	1.25 ± 0.56	0.65 ± 0.075	0.17 ± 0.048

Experimentally measured characteristic times for beads of various diameters performing saltatory motion at saturated surface concentration C_{ss} (see also *inset* in Fig. 3). These times are not defined (*n.d.*) for continuously moving beads. Note that t_s is the time of symmetry breaking; τ' is the characteristic time to polymerize a gel of thickness e^*; τ is the time necessary for the bead to expel from a gel of thickness e^* (see text); and τ_{rep} is the time for the bead velocity to drop from V_{max} to V_{min}. It is also the time needed to start repolymerizing a gel of thickness $\bar{e}$ at a polymerization rate ν_p after the bead was expelled from its surrounding gel (see text). Error in the bead diameter is given by the manufacturer, and the error in the time of symmetry breaking is calculated statistically using 10 beads. Other times were obtained from 15 picks and 3–4 beads.

symmetry of the actin cloud was broken. This time (t_s) is proportional to the bead size (20). From then on, an actin comet was developed and the beads were propelled forward. Two regimes of dynamics were clearly observed—i.e., continuous motion, and saltatory motion—depending on bead size or surface concentration of the activating proteins (Fig. 1). In the continuous regime, the comet developed behind the moving bead is dense and homogeneous except for its first layer (see *inset A* and *C*, Fig. 1), whereas the saltatory regime is characterized by a periodic motion of the beads, a nonconstant velocity cycle, and a nonuniform comet density (see *inset B* and *D*, Fig. 1). In the saltatory regime, the dense and loose parts of the comet are respectively correlated with bead low- and high-speeds, as described in Bernheim-Groswasser et al. (20). From the experimental diagram in Fig. 1 we conclude that the bead movement depends on two controlled variables, the surface density C_s of active actin polymerization activators, and the bead diameter, D. The transition from continuous to saltatory movement can be induced by increasing either the bead diameter D or the protein surface concentration, C_s. One can note that small beads ($D \leq 2.1$ μm) always move continuously regardless of the surface concentration value C_s, whereas larger beads ($2.1 < D < 9.14$ μm diameter) exhibit transitions from saltatory to continuous motion by decreasing C_s. The largest beads in this study, 9.1 μm in diameter, always moved in a saltatory manner in the experimentally investigated domain, $C_s \leq C_{ss} = (6 \pm 1) \times 10^{-2}$ molecules/nm^2, with C_{ss} corresponding to the saturating conditions. The dashed-dot line in Fig. 1 marks the approximate boundary between the two regimes. The critical surface concentration at which the regime changes from continuous to saltatory is a strongly decreasing function of the bead diameter. In addition to the continuous and saltatory regimes, an intermittent regime is identified at a saturating protein surface concentration (C_{ss}) and for an intermediate bead diameter of 2.8 μm (*open triangle* in Fig. 1).

In practice, phase contrast imaging enables us to measure differences in gel density (gray-level) that appear in the comet. If the bead is performing a continuous motion, the only gel density difference is between the first layer and the rest of the comet tail (see *inset A*, Fig. 1). However, if the bead is performing saltatory movement, there are variations in the comet gray-level (see Figs. 1 and 2). In both cases, when the polymerization begins (time $t = 0$), the bead is at rest and a gel layer is built until symmetry is broken (time $t = t_s$) (20). The thickness of this first layer is found to be linearly dependent on the bead diameter (Fig. 2, *triangles*) and regardless of the motion type, whether it is continuous or saltatory. In the case of large beads ($D > 2.1$ μm), which perform discontinuous motion, the following layers are formed while the bead is already in motion: one gel layer is formed during each jump or velocity cycle (*shaded arrows* in Fig. 2). The thickness of these actin gel layers is found to be independent of the bead diameter, its value being $e^* = 1.5 \pm 0.2$ μm (*squares* and *insets a–d* in Fig. 2). One can note from Fig. 2 that the thickness of the first layer is always larger or equal to that of the following ones that are produced during the bead movement.

Experiment analysis (bead velocity, actin gel thickness)

The curvilinear distance traveled by the bead center as a function of time, $X(t)$, was measured using video phase contrast optical microscopy. The velocity $d/dtX(t)$ (time derivative of $X(t)$) was then calculated. The velocity of a 6.3-μm-diameter bead moving in a periodic motion is plotted in Fig. 3. The saltatory motion is characterized by a velocity cycle that starts at a maximal velocity V_{max}, passes through a

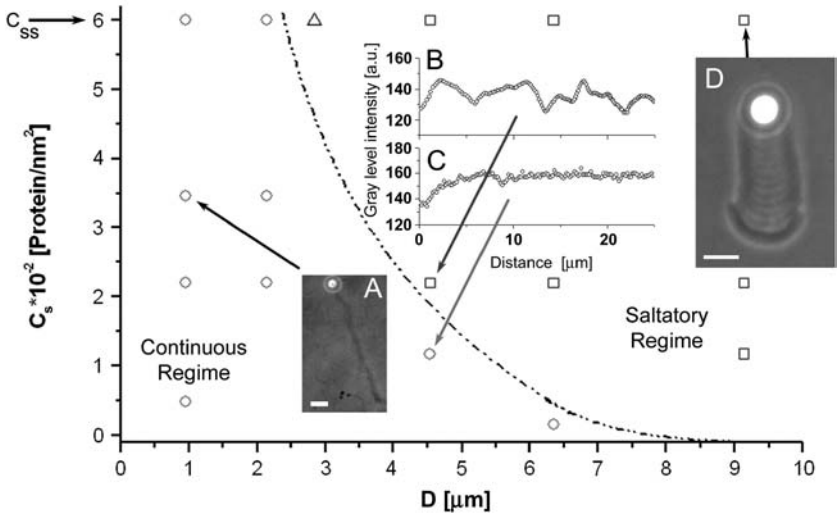

FIGURE 1 A state diagram of the bead dynamics. Two distinct motion regimes are observed depending on the bead diameter D and the protein surface concentration C_s. Insets: (*A*) 1-μm-diameter bead moving continuously, bar = 5 μm; (*B* and *C*) gray-level intensity along the comet for a 4.5-μm-diameter bead at surface concentrations of active proteins of $C_s = (2.2 \pm 0.3) \times 10^{-2}$ molecules/nm^2 and $C_s = (1.17 \pm 0.02) \times 10^{-2}$ molecules/nm^2, respectively; (*D*) 9.1-μm-diameter bead in a saltatory regime, bar = 10 μm. The continuous regime (*open circles*) is characterized by a constant velocity and a constant gel density of the comet tail (*insets A* and *C*). The saltatory regime (*open squares*) is characterized by a periodic movement of the beads and also expressed by a periodic structure of the tail (*insets B* and *D*). The solid dashed-dot line marks the approximate boundary between these two regimes. At a bead diameter of 2.8 μm and at saturating surface concentration $C_s = C_{ss} = (6 \pm 1) \times 10^{-2}$ molecules/nm^2, an intermittent velocity regime (*open triangle*) is identified.

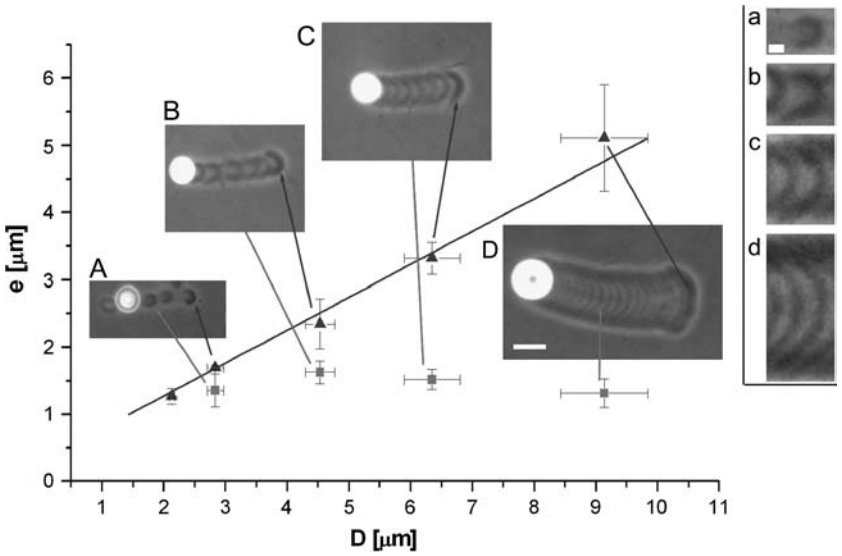

FIGURE 2 Dependence of the thickness of the actin gel layer at symmetry breaking (*triangles*) as a function of the bead diameter D at a saturating surface density C_{ss} of active VCA. The thickness of the first actin burst or layer is found to be linearly dependent on the bead diameter (*triangles*) and regardless of the motion type, whether it is continuous or saltatory. For large beads ($D > 2.1$ μm), which perform discontinuous motion, the following layers are formed while the bead is already in motion, during each jump or velocity cycle (marked by a *shaded arrow*). Insets: the bead diameter is *A* and *a*, 2.8 μm; *B* and *b*, 4.5 μm; *C* and *c*, 6.3 μm; and *D* and *d*, 9.1 μm. (*A–D*) Bar = 10 μm. (*a–d*) Bar = 2 μm. Even though actin depolymerization occurs, the end of the comet remained visible until the end of the experiment. The beads that move periodically display a periodic comet structure (*B–D*, *b–d*). Visual inspection of the structure of the comet body reveals that the thickness of the gel layers is independent of the bead diameter within experimental error (*a–d*). Its value is $e^* = 1.5 \pm 0.2$ μm (*squares*). The gel thickness is measured by analysis of the gray-level intensity of the actin gel along the comet on a final image. The error in the gel thickness is calculated statistically using ~10 beads with ~5 velocity cycles per bead.

minimal velocity V_{min}, and ends at V_{max}. A careful look at a typical velocity cycle starting from V_{max} reveals three phases. The first two phases correspond to a steep decrease of the velocity to V_{min}, followed by a slow increase of the velocity. These two phases are achieved in a total characteristic time τ' (Fig. 3), which is also the time needed for growing a gel of thickness e^*. The third phase is a steep increase of the velocity to V_{max} and corresponds to the expulsion of the bead from the actin shell of thickness e^*. This expulsion phase is achieved in a characteristic time τ (Fig. 3). For different bead sizes, we measured experimentally the characteristic time τ' required for growing a gel of thickness e^* (see Table 1). We found that for beads of large diameter ($D > 2.8$ μm), the time τ' is always smaller than the time of symmetry breaking (t_s), which is the time necessary to built the first layer. Note that this layer is always larger than e^*. In the case of 2.8-μm-diameter beads, t_s equals τ' within experimental error and the thickness of the first layer equals the thickness of the other layers (see also Fig. 2). Additionally, we define as τ_{rep} the time that corresponds to the first phase (steep decrease of the velocity from V_{max} to V_{min}). All times τ', τ, and τ_{rep} are defined in Fig. 3 and their experimental values are given in Table 1.

To analyze the transition from continuous to saltatory movement, we define the velocity amplitude ($V_{max} - V_{min}$).

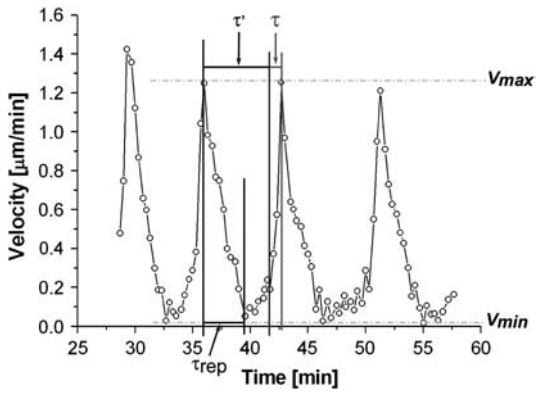

FIGURE 3 Velocity of a 6.3-μm-diameter bead performing periodic motion, as a function of time. During one cycle, there are three phases: *1*, the bead slows down from V_{max} to V_{min}; *2*, the velocity slowly increases to an intermediate velocity; and *3*, the velocity increases abruptly to the value V_{max}. The timelength of each phase is characterized by τ_{rep}, $\tau' - \tau_{rep}$, and τ for phases *1*, *2*, and *3*, respectively.

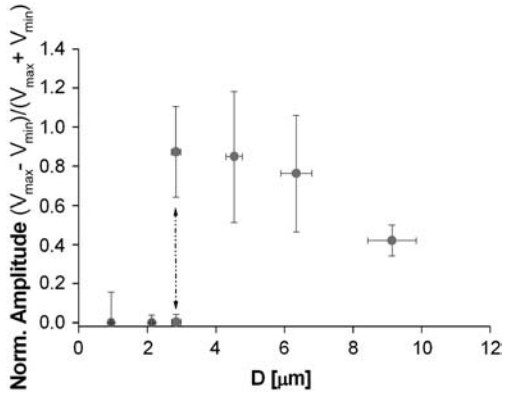

FIGURE 4 The normalized velocity amplitude $(\Delta V/V) = (V_{max} - V_{min})/V_{max} + V_{min})$ as a function of the bead diameter D at saturating surface density C_{ss} is plotted. Small beads ($D \leq 2.1$ μm) move smoothly, thus $(\Delta V/V) = 0$. Increasing the bead diameter ($D \geq 2.8$ μm) induces a transition to a motion type for which $(\Delta V/V) \neq 0$: for intermediate bead diameters ($D = 2.8$ μm) we observe the coexistence of two regimes of motion (*solid dash-dot double arrow*), a steady one, where $(V_{max} - V_{min}) = 0$; and a saltatory one, with $(V_{max} - V_{min}) \neq 0$.

The transition from steady to periodic movement is determined by plotting the normalized velocity amplitude $(\Delta V/V) = (V_{max} - V_{min})/(V_{max} + V_{min})$ as a function of the two control parameters of the system, D or C_s. A typical first-order (discontinuous) transition appears in Fig. 4, where $(\Delta V/V)$ is plotted as function of the bead diameter D for a saturating activator surface density C_{ss}. Small beads ($D \leq 2.1\ \mu$m) move smoothly, thus $(\Delta V/V) = 0$. Increasing the bead diameter ($D \geq 2.8\ \mu$m) induces a transition to a motion type for which $(\Delta V/V) \neq 0$: for intermediate bead diameters ($D = 2.8\ \mu$m) we observe the coexistence of two regimes of motion (*solid dash-dot double arrow* in Fig. 4)—a steady one, where $(V_{max} - V_{min}) = 0$ and a saltatory one, with $(V_{max} - V_{min}) \neq 0$. In that case, the bead movement is intermittent, and shifts randomly from one velocity regime to the other. For larger bead diameters ($D > 2.8\ \mu$m) the movement is always periodic, $(\Delta V/V) \neq 0$, and the velocity amplitude decreases with D (Fig. 4).

DISCUSSION

The transition from continuous to saltatory movement as function of D or C_s (Fig. 1) can be explained by the dimensionless elastic analysis proposed for the mechanism of *Listeria monocytogenes* propulsion (9,10). According to this analysis, the velocity (V) of the bead relative to the gel is given by the balance between the gel elastic propulsion force F_e and the gel/bead surface friction force F_f, at any time. Notations used in the following sections are schemed on Fig. 5.

The elastic force

The elastic force F_e is proportional to the stress integrated over the gel-bead contact area S (9,10). It arises from the necessity of pushing and subsequently extending the already polymerized and cross-linked gel for allowing the insertion of new material at the bead-gel interface. A thorough calculation of the stress would require the use of sophisticated nonlinear elasticity. Yet simple scaling arguments can provide a useful guide for understanding the physical framework of the phenomenon studied here. For the sake of simplicity we adopt this scaling approach here. This stress

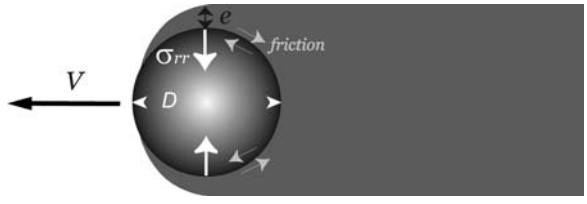

FIGURE 5 Scheme of the notations used in the text. The bead of diameter D is moving at a velocity V and the comet is immobile. The gel layer has a thickness e. Friction occurs between the comet and the bead surface, and the gel elasticity results in a stress σ_{rr} normal to the bead surface.

σ_{rr} depends on the square of the gel thickness e and on the bead diameter D : $\sigma_{rr} \propto Y \times (e/D)^2$, where Y is the elastic modulus of the gel. This formula, used in the case of a nonmoving spherical bead in Noireaux et al. (14), holds as long as deformations are small compared to the radius of curvature. The elastic energy release corresponding to a small displacement δL of the gel relative to the bead is thus $E_{el} \propto Y \times (e/D)^2 \times D \times e \times \delta L$. As a result, the total elastic force scales like the cube of e (21),

$$F_e \propto Y \frac{e^3}{D}. \quad (1)$$

Introducing the elastic force per activator, f_e, we get

$$f_e = F_e \frac{1}{C_s S} \propto Y \frac{e^3}{D^3 C_s}, \quad (2)$$

where the surface area S is the contact surface between the actin gel and the bead surface, proportional to D^2. Details of the expression of the elastic modulus Y as a function of the actin filaments bending modulus and the average distance between crosslinks in the gel can be found in Head et al. (23). Note that Eqs. 1 and 2 are scaling relations involving unknown coefficients depending only on geometric factors. The comprehension of the dependence of the gel thickness e on the bead diameter D and on the relative velocity V will enable us to find the dependence of the elastic force on these two parameters.

A complete analysis of the bead movement must include a description of the polymerization dynamics during a complete velocity cycle. From Eq. 2 one finds that the propulsion force increases with the gel thickness e. Since the maximal value of e is found experimentally to be independent of the bead size $e = e^* = 1.5 \pm 0.2\ \mu$m (Fig. 2), the maximal value of the elastic force reads

$$f_{e*} \propto Y \frac{e^{*3}}{D^3 C_s}. \quad (3)$$

As a result, the value of f_{e*} depends only on the size of the bead and on the surface density C_s of the activating protein, and is independent of the velocity V. We assume that this result is also valid for f_e that is thus independent of V.

The friction force

There are two contributions to the friction between the bead and the gel: one is the standard contact surface friction, which is simply proportional to the bead-gel relative velocity and the contact area. It is described by a constant surface friction coefficient, ξ_s. Such a term always exists: it results either from the direct friction of the filaments on the solid surface, or from the indirect friction transmitted by the fluid to the solid surface. The second term is more subtle, and results from the existence of a finite average time over which an actin filament is bound to an activator, or, in other terms, to transient attachments to the surface of the bead (8,9). It is

proportional to the friction area, the protein surface density C_s, and the average force between an actin filament and an actin polymerization activator, $\tilde{f}_f$. Hence the total friction force, F_f can be written as (9,10)

$$F_f = \left(C_s \tilde{f}_f + \xi_s V\right) S, \tag{4}$$

where S is the area of the contact surface between the bead and the comet.

Per actin polymerization activator, the friction force can be expressed as

$$f_f = \frac{F_f}{C_s S} = \tilde{f}_f + \frac{\xi_s}{C_s} V. \tag{5}$$

One can note that f_f is independent of the bead size, and the contact surface. The average force $\tilde{f}_f$, and thus f_f, depend on V in a nontrivial way (9,10), as sketched in Fig. 6:

1. At small velocities (segment *a-b* in Fig. 6), $\tilde{f}_f$ is proportional to V with a coefficient that we denote α ($\tilde{f}_f \approx \alpha V$); and a large friction coefficient per nucleator, $\gamma = (\alpha + (\xi_s/C_s))$ can be defined ($f_f = \gamma V$) (equivalently, if we note β the friction coefficient, the friction force per unit surface reads $C_s \gamma V = \beta V$).
2. At large velocities (segment *c-d* in Fig. 6), bonds break in a time proportional to the velocity V, and $\tilde{f}_f$ is inversely proportional to the bead velocity: $\tilde{f}_f \alpha\, 1/V$. Thus at large velocities, $\tilde{f}_f$ vanishes and the only contribution to the friction force comes from the standard friction ξ_s.

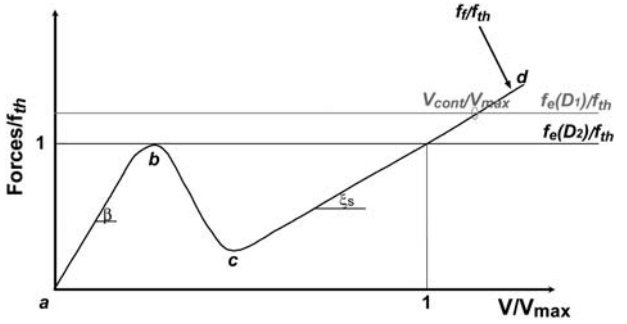

FIGURE 6 Schematic plot of the normalized elastic force per nucleator f_e/f_{th} and the normalized friction force $f_f(V)/f_{th}$ as a function of the normalized bead velocity V/V_{max} for two different bead diameters D_1 and D_2 ($D_1 \leq D_2$). The elastic force f_e is independent of V (see text). The normalized friction force curve has a complex velocity dependence: at low (*a-b* branch) and high (*c-d* branch) velocities, the normalized friction force is proportional to the velocity with a large (coefficient β) and a standard (coefficient ξ_s) friction coefficient per nucleator, respectively. For intermediate velocities (segment *b-c*), the dependence on V is non-monotonous. The force normalization quotient f_{th} corresponds to the local maximum of the friction curve and also to the elastic force threshold that delimits the saltatory and continuous regimes. When the two curves intersect at a single point, we are in the continuous regime of motion, characterized by a velocity V_{cont}/V_{max}. When there are two intersection points (at $f_e \cong f_{th}$ for $e = e^*$, point *b* and point *1,1*), we are in the saltatory regime. Note that an increase of D from D_1 to D_2 reduces the propulsion force and drives the system toward a saltatory regime of motion.

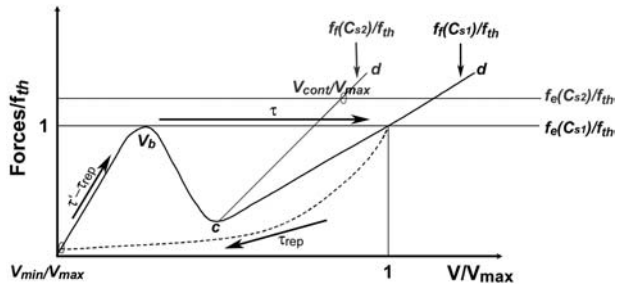

FIGURE 7 Schematic plot of the normalized elastic force per nucleator f_e/f_{th} and the normalized friction force $f_f(V)/f_{th}$ as a function of the normalized bead velocity V/V_{max} for two different protein surface concentrations C_{s1} and C_{s2} ($C_{s1} > C_{s2}$). The force normalization quotient f_{th} corresponds to the maximal value of the force for the first friction branch, and also to the force threshold that delimits the saltatory and the continuous regimes. Starting from a surface concentration $C_s = C_{s2}$ and a bead diameter such that the movement is in a continuous regime (one intersection point at abscissa V_{cont}/V_{max}) and increasing C_s to C_{s1} leads to a saltatory motion characterized by the two extreme velocities V_{max} and V_{min}. The characteristic time τ_{rep} is the typical time during which the velocity drops from V_{max} to V_{min} (*dashed curve*), it also corresponds to the time required to repolymerize a gel of thickness $\bar{e}$ after being expelled from the bead surface. The value τ' is the time it requires to rebuild a gel of thickness e^*. It also corresponds to the time it takes for the velocity to drop from V_{max} to V_{min} (*dashed line*) and to accelerate again to an intermediate velocity V_b. The time $\tau' - \tau_{rep}$ represents the typical time for the gel to continue building up a gel from thickness $\bar{e}$ to e^* and the bead velocity to accelerate from V_{min} to V_b. Finally, τ is the time it takes to expel the gel of thickness e^* from the bead surface, where the velocity during this period accelerate from V_b to V_{max} (*horizontal arrow*). The duration of one complete velocity cycle is therefore $\tau' + \tau$.

3. For intermediate velocities (segment *b-c* in Fig. 6), a non-monotonous dependence of $f_f(V)$ on V is expected.

Note that the first branch slope is higher than the second branch slope ($\gamma C_s > \xi_s$), due to the fact that fewer bonds are present between the bead and the actin gel in the second branch.

Analysis of the bead movement

The bead velocity is determined by the balance between the elastic force f_e and the friction force $f_f(V)$ (in Fig. 6 and Fig. 7 these forces are normalized by the threshold force f_{th} defined below; also the velocities are normalized by the maximal velocity V_{max}). Whenever the intercept of the two curves is far from the non-monotonous region of the $f_f(V)$ curve, the expected behavior is a simple steady motion (continuous regime), characterized by the velocity V_{cont}, which is that of the intersection point (i.e., intercept of $f_f(V)$ and $f_e(D_1)$ in Fig. 6 and intercept of $f_f(C_{s2})$ and $f_e(C_{s2})$ in Fig. 7). When the intercept is close to the non-monotonous region of $f_f(V)$, the motion type cannot be directly deduced from our former analysis and depends on how fast the gel layer grows, while being expelled from the bead. In other words, when the elastic force f_e barely exceeds the threshold value f_{th} (Figs. 6 and 7), the friction drops abruptly and the gel layer is

expelled from the bead in a characteristic time τ. If τ is long compared to the time τ' required for growing a gel layer around the bead, this gel layer is maintained, the system is at steady state and the bead motion is continuous at a constant velocity V_{cont} (Fig. 7). In the continuous regime, it is difficult to obtain an exact experimental estimate of the gel thickness around the bead. However, we observe that this thickness is not larger than the 1.5-μm thickness that corresponds to e^* (see, for example, the continuous regime bead of Fig. 1). If τ is short compared to τ', the consequence will be the appearance of a saltatory motion where $f_e \cong f_{th}$ (see $f_f(V)$ and $f_e(D_2)$ in Fig. 6 and $f_f(C_{s1})$ and $f_e(C_{s1})$ in Fig. 7). For saltatory motion, a velocity cycle that starts at a maximal velocity V_{max} passes through a minimal velocity V_{min}, and ends at V_{max}. Rough estimates of the times τ and τ' gives $\tau \cong D/V_{max}$ and $\tau' \cong e^*/\nu_p$ (where ν_p is the velocity of polymerization on the bead surface). The condition for obtaining a saltatory motion is thus $V_{max} \gg \nu_p D/e^*$. Given that $D > e^*$ (see Fig. 2), the maximal velocity is always greater than the polymerization velocity. This is in agreement with our experiments since the maximal velocity is of the order of 1 μm/min (20), whereas the polymerization velocity (24) is lowered in the presence of stress (14).

According to the discussion of the preceding section, the increase in bead diameter D decreases the propulsion force per nucleator f_e (Eq. 3) without changing the friction term f_f. Thus, varying D at constant nucleator surface concentration opens the possibility to investigate the state diagram of the system dynamics. The fact that small beads move at a relatively high constant velocity ($\sim$1 μm/min) is in agreement with the theoretical analysis of the force-velocity curve depicted in Fig. 6. One can see that the intersection of the elastic force $f_e(D_1)$ with the fast branch of the friction force $f_f(V)$ (*c-d* segment) results in a high and constant velocity. The increase of D reduces the propulsion force and drives the system toward the saltatory regime ($f_f(V)$ and $f_e(D_2)$ *curves*, Fig. 6) as observed experimentally (Figs. 1 and 4).

Conversely, varying the surface nucleator concentration at constant bead diameter also allows exploring the system state diagram. At a given velocity, the friction force per nucleator decreases when the nucleator density is increased: $\tilde{f}_f$ is independent of C_s, whereas the second term of Eq. 5 is inversely proportional to C_s. As a consequence, the slope of the *c-d* part is a decreasing function of C_s, as shown in Fig. 7.

The C_s dependence of the propulsion force is difficult to assess. A naive analysis would predict an increase of the elastic modulus with C_s. However, under strong branching conditions controlled by the Arp2/3 complex, the elastic modulus Y should become essentially independent of C_s. Thus the propulsion force per activator should increase upon decreasing C_s. Thus, starting from a saltatory regime and decreasing C_s at constant D should lead the system to a continuous regime according to Fig. 7. Note that the stationary velocity V_{cont} in the continuous regime is smaller than the maximal velocity V_{max} in the saltatory regime in a suitable parameter range. This corresponds to our experimental observations, since V_{max}/V_{cont} is 2.6 and 4.3 for 6.3-μm-diameter beads coated with $0.37 \times C_{ss}$ and $0.02 \times C_{ss}$ proteins, respectively, and 1.8 for 4.5-μm-diameter beads coated with $0.195 \times C_{ss}$ proteins.

Analysis of the saltatory regime and numerical estimates

In a velocity cycle, the maximal velocity is obtained for the smallest friction force. Considering the simple argument that the new actin gel is in a triangle defined by ℓ and e^*, where the gel moves parallel to the bead surface (see Fig. 8), we find that ℓ equals $V_{max}/\nu_p e^*$. Under these conditions the total friction force applies on a surface of the order of $D \times \ell$, hence

$$F_f \approx \xi_s D \times \ell \times V_{max} \approx \xi_s V_{max}^2 e^* \frac{D}{\nu_p}. \quad (6)$$

This is obtained by assuming that the polymerization velocity does not depend on the local stress. A more complete analysis would require taking this effect into account. The coefficient ξ_s is the constant surface friction coefficient corresponding to the fast branch of the friction force curve (*c-d* segment of $f_f(V)$, Fig. 6). The maximal velocity V_{max} can now be deduced by equating F_f to the total propulsion force $F_{e^*} \propto Ye^{*3}/D$ *at* $e = e^*$ (see Eq. 1):

$$V_{max} \approx \sqrt{V_p \frac{Y}{\xi_s} \frac{e^*}{D}}. \quad (7)$$

This linear dependence of V_{max} on $1/D$ is in qualitative agreement with our observations for beads performing saltatory movement (see Fig. 9).

The minimal velocity V_{min} can be estimated by calculating the friction force on the *a-b* segment of $f_f(V)$ (Figs. 6 and 7). The total friction force is given by $\beta D^2 V_{min}$, where $\beta = \gamma C_s$ is the friction coefficient and D^2 is the bead-gel friction area. The minimal velocity V_{min} results from the balance between the total friction force $\beta D^2 V_{min}$ and the total elastic propulsion force $Y\bar{e}^3/D$ where $\bar{e}$ is the gel thickness around the bead when it is propelled at the velocity V_{min}. The value of $\bar{e}$ is not accessible directly from our experiments. How-

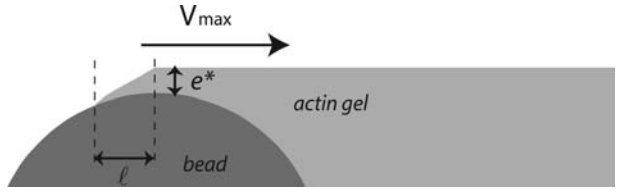

FIGURE 8 Scheme: characteristic length ℓ over which the relative velocity of the gel as referenced to the bead is V_{max}. The friction is then at its minimum value. During the same time τ', the thickness e^* polymerizes at the velocity of polymerization ν_p, and the gel advances on the length ℓ at a velocity V_{max}. Thus we obtain $\tau' \cong e^*/\nu_p = \ell/V_{max}$.

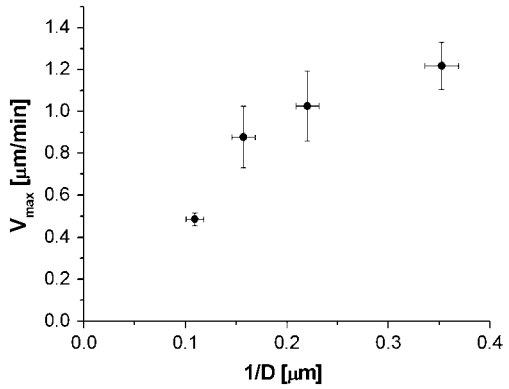

FIGURE 9 The maximal velocity V_{max} of beads performing periodic motion at saturating protein surface density is plotted as a function of inverse bead diameter (D^{-1}).

ever, we can measure the time τ_{rep} necessary to repolymerize a gel of thickness $\bar{e}$ at a polymerization rate ν_p after the bead was expelled from its surrounding gel, and $\bar{e} = \tau_{rep}\nu_p$. The time τ_{rep} corresponds also to the time necessary for the velocity to drop from its maximal value V_{max} to its minimum value V_{min} (see Figs. 3 and 7). The minimal velocity V_{min} is thus given as a function of τ_{rep} by equating the friction and propulsion forces:

$$V_{min} \approx \frac{Y}{\beta}\frac{\tau_{rep}^3\nu_p^3}{D^3}. \quad (8)$$

We can use the expression for τ', the time required to develop a gel of thickness e^*, $\tau' \cong e^*/v_p$, to express the minimal velocity in terms of the measurable parameters e^*, D, τ_{rep}, and τ':

$$V_{min} \approx \left(\frac{Y}{\beta}\right)\frac{e^{*3}}{D^3}\frac{\tau_{rep}^3}{\tau'^3}. \quad (9)$$

In practice we find that $\tau \ll \tau_{rep} < \tau'$ (see Table 1) and since the ratio of $e^*/D < 1$ for all bead diameters studied, then $(e^{*3}/D^3)(\tau_{rep}^3/\tau'^3) \ll 1$. Taking all these parameters into account, we evaluate V_{min} to be almost zero, again in agreement with our experimental results. The ratio Y/β in Eq. 9 represents a characteristic velocity: under stretching conditions, if the bead velocity is greater than Y/β, the elastic force is dominant, whereas for velocities smaller than Y/β, the friction dominates (25). The value of Y/β can be estimated from our experimental data as follows: the minimal velocity for a bead of diameter $D = 2.8$ μm is $V_{min} = 0.082$ μm/min, where $e^*/D \approx 1/2$ (see Fig. 2) and $\tau_{rep}/\tau' \approx 0.7$ (Table 1); therefore $Y/\beta \approx 0.015$ μm/min. With Y of the order of 10^3–10^4 Pa (25,26), the friction coefficient β is equal to 4×10^{13} Pa s/m, or 4 pN/nm. Since the surface concentration of activating proteins is of the order of 10^{-2} mol/nm^2 (see Materials and Methods, above), the value of β is of 4 pN $\times$ s $\times$ nm^{-1}. Thus, in the slow regime motion, the tangential force exerted on average per filament on the bead is of the order of a few pN, which is quite reasonable.

CONCLUSION

We investigated a simple experimental system for the study of the mechanism of actin-based propulsion to highlight the role of physical parameters at a mesoscopic scale. The state diagram of the system dynamics was studied as a function of the size of the beads and of the surface concentration of actin nucleators. Two distinct regimes of motion are observed—saltatory and continuous. The transition from one regime to the other is described with the use of a mesoscopic analysis that involves elastic and friction forces, and uses experimental estimates. A non-monotonous dependence of the friction as a function of the bead velocity explains the oscillatory behavior of the movement and well describes the experimental observations such as velocities and characteristic times. Its virtue is to cast the description of actin-based motility in a few parameters, which can be related to molecular mechanisms and measured experimentally.

We thank Marie-France Carlier for the gift of the motility medium, Sebastian Wiesner for his help in measuring the activity of the proteins immobilized on the surfaces, and Julie Plastino for her help on the experimental setup. We thank Franck Jülicher and Ken Sekimoto for many fruitful discussions.

REFERENCES

1. Taunton, J., B. A. Rowning, M. L. Coughlin, M. Wu, R. T. Moon, T. J. Mitchison, and C. A. Larabell. 2000. Actin-dependent propulsion of endosomes and lysosomes by recruitment of N-WASp. *J. Cell Biol.* 148:519–530.
2. Merrifield, C. J., S. E. Moss, C. Ballestrem, B. A. Imhof, G. Giese, I. Wunderlich, and W. Almers. 1999. Endocytic vesicles move at the tips of actin tails in cultured mast cells. *Nat. Cell Biol.* 1:72–74.
3. Theriot, J. A., T. J. Mitchison, L. G. Tilney, and D. A. Portnoy. 1992. The rate of actin-based motility of intracellular *Listeria monocytogenes* equals the rate of actin polymerization. *Nature.* 357:257–260.
4. Egile, C., T. P. Loisel, V. Laurent, R. Li, D. Pantanoli, P. J. Sansonetti, and M.-F. Carlier. 1999. Activation of the CDC42 effector N-WASp by the *Shigella flexneri* IcsA protein promotes actin nucleation by Arp2/3 complex and bacterial actin-based motility. *J. Cell Biol.* 146:1319–1332.
5. Machesky, L. M., R. D. Mullins, H. N. Higgs, D. A. Kaiser, L. Blanchoin, R. C. May, M. E. Hall, and T. D. Pollard. 1999. SCAR, a WASp-related protein, activates nucleation of actin filaments by the Arp2/3 complex. *Proc. Natl. Acad. Sci. USA.* 96:3739–3744.
6. Pistor, S., T. Chakraborty, K. Niebuhr, E. Domann, and J. Wehland. 1994. The ActA protein of *Listeria monocytogenes* acts as a nucleator inducing reorganization of the actin cytoskeleton. *EMBO J.* 13:758–763.
7. Mogilner, A., and G. Oster. 1996. Cell motility driven by actin polymerization. *Biophys. J.* 71:3030–3045.
8. Mogilner, A., and G. Oster. 2003. Force generation by actin polymerization. II. The elastic ratchet and tethered filaments. *Biophys. J.* 84:1591–1605.

9. Gerbal, F., V. Noireaux, C. Sykes, F. Jülicher, P. Chaikin, A. Ott, J. Prost, R. M. Golsteyn, E. Friederich, V. Louvard, V. Laurent, and M. F. Carlier. 1999. On the *Listeria* propulsion mechanism. *Pramana J. Phys.* 53:155–170.
10. Gerbal, F., P. Chaikin, Y. Rabin, and J. Prost. 2000. An elastic analysis of *Listeria monocytogenes* propulsion. *Biophys. J.* 79:2259–2275.
11. Carlsson, A. E. 2001. Growth of branched actin networks against obstacles. *Biophys. J.* 81:1907–1923.
12. Carlsson, A. E. 2003. Growth velocities of branched actin networks. *Biophys. J.* 84:2907–2918.
13. Cameron, L. A., J. R. Robbins, M. J. Footer, and J. A. Theriot. 2004. Biophysical parameters influence actin-based movement, trajectory, and initiation in a cell-free system. *Mol. Biol. Cell.* 15:2312–2323.
14. Noireaux, V., R. M. Golsteyn, E. Friederich, J. Prost, C. Antony, D. Louvard, and C. Sykes. 2000. Growing an actin gel on spherical surfaces. *Biophys. J.* 278:1643–1654.
15. Lasa, I., E. Gouin, M. Goethals, K. Vancompernolle, V. David, J. Vandekerckhove, and P. Cossart. 1997. Identification of two regions in the amino terminal domain of ActA involved in the actin comet tail formation by *Listeria monocytogenes*. *EMBO J.* 16:1531–1540.
16. Cameron, L. A., M. J. Footer, A. Van Oudenaarden, and J. A. Theriot. 1999. Motility of ActA protein-coated microspheres driven by actin polymerization. *Proc. Natl. Acad. Sci. USA.* 96:4908–4913.
17. Upadhyaya, A., J. R. Chabot, A. Andreeva, A. Samadani, and A. van Oudenaarden. 2003. Probing polymerization forces by using actin-propelled vesicles. *Proc. Natl. Acad. Sci. USA.* 100:4521–4526.
18. Giardini, P. A., D. A. Fletcher, and J. A. Theriot. 2003. Compression forces generated by actin comet tails on lipid vesicles. *Proc. Natl. Acad. Sci. USA.* 100:6493–6498.
19. Loisel, T. P., R. Boujemaa, D. Pantaloni, and M. F. Carlier. 1999. Reconstitution of actin-based motility of *Listeria* and *Shigella* using pure proteins. *Nature.* 401:613–616.
20. Bernheim-Groswasser, A., S. Wiesner, R. M. Golsteyn, M.-F. Carlier, and C. Sykes. 2002. The dynamics of actin-based motility depend on surface parameters. *Nature.* 417:308–311.
21. Prost, J. 2001. The physics of *Listeria* propulsion. *In* Physics of Biomolecules and Cells. H. Flyvbjerg, F. Julicher, P. Ormos, and F. David, Springer, Les Houches, France. 215–236.
22. Fradelizi, J., V. Noireaux, J. Plastino, B. Menichi, D. Louvard, C. Sykes, R. M. Golsteyn, and E. Friederich. 2001. ActA and human zyxin harbour Arp2/3-independent actin-polymerization activity. *Nat. Cell Biol.* 3:699–707.
23. Head, D. A., A. J. Levine, and F. C. MacKintosh. 2003. Distinct regimes of elastic response and deformation modes of cross-linked cytoskeletal and semiflexible polymer networks. *Phys. Rev. E.* 68: 061907.
24. Amann, K. J., and T. D. Pollard. 2001. Direct real-time observation of actin filament branching mediated by ARP2/3 complex using total internal reflection fluorescence microscopy. *Proc. Natl. Acad. Sci. USA.* 98:15009–15013.
25. Marcy, Y., J. Prost, M.-F. Carlier, and C. Sykes. 2004. Forces generated during actin-based propulsion: a direct measurement by micromanipulation. *Proc. Natl. Acad. Sci. USA.* 101:5993–5997.
26. Gerbal, F., V. Laurent, A. Ott, M.-F. Carlier, P. Chaikin, and J. Prost. 2000. Measurement of the elasticity of the actin tail of *Listeria monocytogenes*. *Eur. Biophys. J.* 29:134–140.